Performance Comparison of the Target Detection Methods in High Speed Platform Forward Looking SAR (HSP-FLSAR)

S. M. Hosseini Miangafsheh, M. Kazerooni, M. Abolghasemi
Faculty of Electrical & Computer Engineering, Malek Ashtar University of Technology, Iran
smhoseinie@mut.ac.ir, kazerooni@mut.ac.ir, abolghasemi@mut.ac.ir
Corresponding author: kazerooni@mut.ac.ir

***Abstract*- Sea target detection in the HSP-FLSAR images has not been addressed so far in the literature. In this paper we carry out a comparative evaluation of existing SAR target detection algorithms in the case of monostatic HSP-FLSAR range Doppler images assuming a platform diving trajectory. To do so, various CFAR methods, including CA-CFAR, SOCA-CFAR, GOCA-CFAR, OS-CFAR, VIE-CFAR, and G0 distribution CFAR algorithms, are used to detect a set of point scatterers in simulated images. The performance of methods is compared based on receiver operating characteristic curves. Simulation results show that OS-CFAR has the best probability of detection for a fixed probability of false alarm. This paper can be a starting point to find better target detection methods in HSP-FLSAR images.**

***Index Terms*-** CFAR, Forward Looking SAR, High Speed Platform, Target Detection.

I. INTRODUCTION

All weather, day and night operation of the SAR imaging system makes it a powerful tool for many applications. However, monostatic forward looking SAR (FLSAR) has not been widely used due to limited azimuth resolution and left-right ambiguity. But research in monostatic FLSAR field is still ongoing because of simplicity and standalone operation compared to bistatic and linear array FLSAR [1]-[2]. One of the applications of FLSAR is to provide an image of the sea surface for terminal scene matching and guidance of high speed platforms (HSPs) [3]. So, finding an appropriate target detection algorithm in HSP-FLSAR images is necessary.

Target detection in monostatic FLSAR has not been addressed in the literature. But due to the similarity between FLSAR and side looking SAR, we review detection algorithms in side looking

Manuscript received 15-Feb.-2021 and revised 29-May-2021,
Accepted on 18- June-2021
P- ISSN: 2322-4088
E- ISSN: 2322-3936

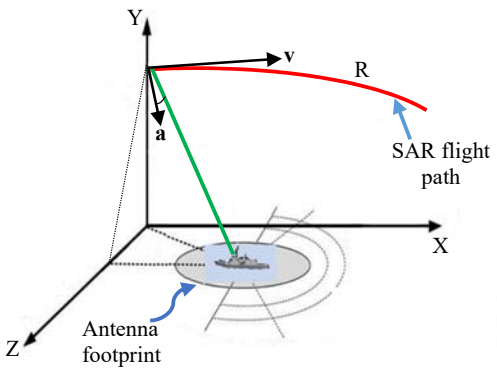

Fig. 1. HSP-FLSAR imaging geometry, **a** and **v** are platform acceleration and velocity vectors

SAR. Target detection methods, especially in the marine field, mostly focus on the CFAR algorithm and its variations [4].

CFAR can optimize the probability of detection while holding the false alarm rate almost constant. The main idea of CFAR is that ships in SAR images appear as bright pixels, which is statistically different from their surrounding area, namely clutter. The simplest forms of CFAR are CA-CFAR and 2P-CFAR, which assume a negative exponentially and Gaussian distribution models for clutter, respectively [5]. They are good in homogenous clutter, but their performance degrades in nonhomogeneous environments. Other algorithms are designed to overcome nonhomogeneous clutter. The smallest of CA-CFAR (SOCA-CFAR) has good performance in multitarget situation but unacceptable in clutter edges. The greatest of CA-CFAR (GOCA-CFAR) performs well in clutter edges but degrades in homogeneous clutter. OSCFAR can handle clutter statistics corruption by interfering targets, but it performs worse in homogeneous clutter [6].

To avoid the disadvantages of different methods, some adaptive algorithms are introduced which can automatically switch between them based on clutter conditions. VIE-CFAR uses a variability index and a mean ratio in the leading and lagging sections of the CFAR window to remove variable cells from the calculation of the CA-CFAR parameter or switch between CA-CFAR and GOCA-CFAR [7]. It also proposes an excision procedure to eliminate the masking effect of interfering targets on both sides of the CFAR window.

Accurate statistical modelling of clutter has great significance in CFAR target detection performance. So a number of papers deal with clutter statistics modelling [8]-[9].

In this paper, range Doppler domain target detection in a monostatic HSP-FLSAR is considered. The SAR platform has a diving trajectory. Fig. 1 shows the imaging system geometry. We consider

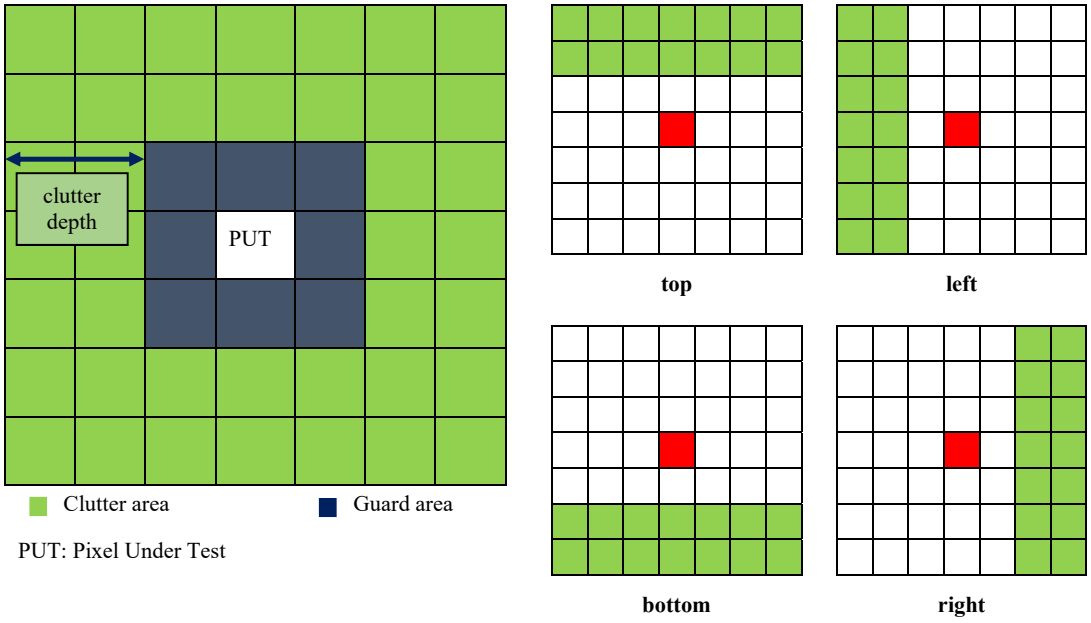

Fig. 2. (a) CFAR window, (b) top, bottom, left, and right parts of CFAR window

some traditional CFAR methods and also some newer detection algorithms. Our goal is to be a starting point for finding the best detection method in HSP-FLSAR marine target detection. So the paper is organised as follows. In section II various detection methods are introduced. Then, detection results on simulated images and some discussions are given in section III. Finally, conclusions are drawn in section IV.

II. DETECTION METHODS

Seeking to find the best method of sea target detection in a monostatic HSP-FLSAR, we investigated a variety of existing detection algorithms. The CFAR method and its variations are dominant in the field of SAR target detection. The simplest version of CFAR is to compare each pixel in the image with a threshold and determine whether the pixel is part of a target or clutter [5].

$$x_{PUT} \begin{cases} > \alpha T & \Rightarrow \ target \\ < \alpha T & \Rightarrow \ clutter \end{cases} \tag{1}$$

Where x_{PUT} is the intensity of pixel under test, T is method parameter and α is a factor which depends on the clutter probability distribution function. The whole image is scanned by a the CFAR window. The CFAR window, which is depicted in Fig. 2, shows a pixel under test surrounded by a guard and

clutter areas. Cell averaging CFAR or CA-CFAR assumes an exponential distribution for clutter so the parameter α is calculated by relation (2).

$$\alpha_{CA} = N_c (P_{fa}^{-1/N_c} - 1) \tag{2}$$

Where P_{fa} is the probability of false alarm, N_c is the number of clutter pixels, and T is the average of clutter pixels [10]. In two-parameter CFAR clutter is modelled by Gaussian distribution with mean and variance parameters of μ and σ [11]. The threshold can be obtained by relation (3)

$$P_{fa} = \frac{1}{2} - \frac{1}{2} erf\left(\frac{Th - \mu}{\sigma\sqrt{2}}\right) \tag{3}$$

Where is Th threshold and $erf(.)$ is error function. SOCA-CFAR uses equation (4) to compute α_{SO} [12].

$$P_{fa}/2 = (2 + \frac{\alpha_{SO}}{N_c/2})^{-N_c/2} \times \left\{ \sum_{k=0}^{N_c/2-1} \binom{N_c/2 - 1 + k}{k} (2 + \frac{\alpha_{SO}}{N_c/2})^{-k} \right\} \tag{4}$$

The T Parameter is the smallest arithmetic mean of the top, bottom, left, and right parts of the clutter area. For GOCA-CFAR the parameter α_{GO} is calculated by equation (5).

$$P_{fa}/2 = (1 + \frac{\alpha_{GO}}{N_c/2})^{-N_c/2} - (2 + \frac{\alpha_{GO}}{N_c/2})^{-N/2} \times \left\{ \sum_{k=0}^{N_c/2-1} \binom{N_c/2 - 1 + k}{k} (2 + \frac{\alpha_{GO}}{N_c/2})^{-k} \right\} \tag{5}$$

And the T parameter is the largest mean of the top, bottom, left, and right parts of the clutter area. In OS-CFAR method T is the 75th order statistics of clutter pixels and α_{OS} is obtained by relation (6) [12].

$$P_{fa} = k \binom{N_c}{k} \frac{\Gamma(\alpha_{OS} + N_c - k + 1)}{\Gamma(\alpha_{OS} + N_c + 1)} = \prod_{i=N_c-k+1}^{N_c} \frac{i}{\alpha_{OS} + i} \tag{6}$$

The value of α in relations (4), (5), and (6) is calculated by numerical iterations, but in order to reduce the computational cost, one can calculate it for different sizes of the CFAR window and different values of P_{fa} and store it in memory.

VIE-CFAR method uses two intelligent switches to combine the advantages of the

abovementioned algorithms [7]. The first switch is the variability index or VI , which is defined by relation (7)

$$VI = 1 + \frac{\hat{\sigma}^2}{\hat{\mu}^2} = 1 + \frac{1}{N_c - 1} \sum \frac{(x_i - \bar{x})^2}{(\bar{x})^2} \tag{7}$$

Where $\hat{\sigma}^2$ is variance, $\hat{\mu}$ is mean and $\bar{x}$ is the arithmetic mean of clutter pixels. VI is different in homogenous and heterogeneous clutters, so the variability of clutter can be recognised. The second switch is the mean ratio or MR which is defined by relation (8)

$$MR = \frac{\bar{x}_A}{\bar{x}_B} = \frac{\sum_{i \in A} x_i}{\sum_{i \in B} x_i} \tag{8}$$

$\bar{x}_A$ and $\bar{x}_B$ are the arithmetic means of the lead and lag parts of CFAR window. MR can be used to detect clutter edges in a single CFAR window. There is an excision procedure in this method which can suppress the masking effect of interfering targets on both sides of the CFAR window.

CFAR method greatly depends on clutter statistical modelling. So many clutter probability distribution functions have been introduced and investigated. One of them, which is perfect to some extent, is G^0 distribution. The relation of G^0 probability distribution function is as follows [13]:

$$G^0(\alpha, \gamma, n) = \frac{n^n \Gamma(n - \alpha) x^{n-1}}{\gamma^\alpha \Gamma(n) \Gamma(-\alpha) (\gamma + nx)^{n-\alpha}} \quad -\alpha, \gamma, n, x > 0 \tag{9}$$

x is pixel intensity, n is the equivalent number of looks, α is the clutter shape parameter, γ is the clutter scale parameter, and $\Gamma(.)$ is gamma function. Parameter α indicates the homogeneity of clutter and it can model homogeneous to extremely heterogeneous clutters. Two main problems of each clutter modelling are the parameter estimation and the calculation of the detection threshold value. The method of moments, Mellin transform, and some hybrid algorithms are existing parameter estimation methods of G^0 distribution [14]. Here, for simplicity, the method of moments is considered. The kth order moments of G^0 distribution can be expressed as

$$E(x^k) = \left(\frac{\gamma}{n}\right)^k \frac{\Gamma(n + k)}{\Gamma(n)} \frac{\Gamma(-\alpha - k)}{\Gamma(-\alpha)} \tag{10}$$

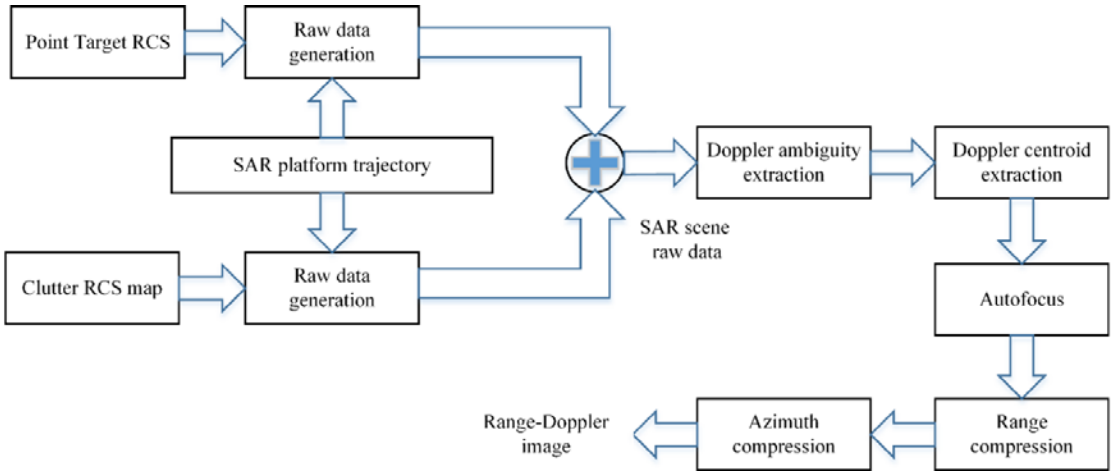

Fig. 3. SAR image simulation block diagram

Table I. SAR image simulation parameters

parameter	value
Carrier frequency	X band
polarization	HH
Target azimuth shift	2000 m
Target range shift	2000 m
Platform velocity	6 Mach
Slant range	50 km
Angle of incidence	50 degree

Assuming n =1 parameters α and γ can be obtained as follows:

$$\alpha = -1 - \frac{E(x^2)}{E(x^2) - 2E^2(x)}$$
$$\gamma = -(\alpha + 1)E(x) \tag{11}$$

Also, there is a closed form relation for the threshold level.

$$Th = \gamma(P_{fa}^{1/\alpha} - 1) \tag{12}$$

III. SIMULATION RESULTS

In order to evaluate detection algorithms, we use simulated images [15]. Fig. 3 shows the block diagram of the simulation method. Raw data is generated for target and clutter separately and finally added to each other to obtain a SAR scene. After that, platform speed is estimated by Doppler

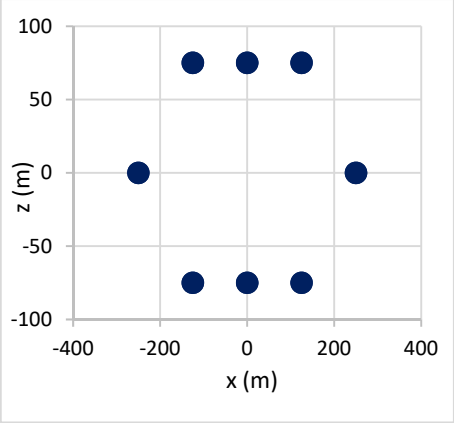

Fig. 4. Target point scatterers

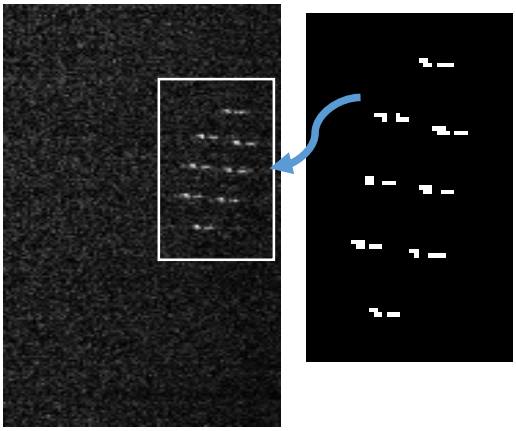

Fig. 5. Simulated SAR image

centroid extraction and then, through autofocus, range compression, and azimuth compression stages, the SAR scene range Doppler image is generated.

Simulation parameters are provided in Table I. Fig. 4 depicts the target which is a set of point scatterers. It is assumed that the target center has a 2000 meter shift along range and azimuth. The simulated image is shown in Fig. 5. Only part of the image is shown here for clarity. Point targets have different ranges and Dopplers related to the SAR platform, so the target image is a little skewed. Also, due to the SAR platform diving trajectory and non-ideal focusing of the imaging method, a single point scatterer spreads to several pixels in the simulated image, as depicted in Fig. 5. So it tends to be 62 pixels as the target in the SAR image. We use this image as an input to the target detection stage.

All the detection algorithms of section 2 are implemented in software. Fig. 6 shows the detection results of CA-CFAR, 2P-CFAR, SOCA-CFAR, GOCA-CFAR, OS-CFAR, VIE-CFAR, and G0-CFAR methods. Also, values of probability of detection, probability of false alarm, and figure of merit of each method are listed in table II. The SOCA-CFAR is eliminated here for its poor results. The actual size of the simulated image in Fig. 5 is 2845×618 pixels, so the total number of clutter pixels or N_c is equal to 1758210. The probability of detection is defined as [16]

$$P_d = \frac{N_d}{N_t} \tag{13}$$

Where N_d is the number of target pixels that have been correctly detected and N_t is the real number of target pixels. Also, the probability of false alarm is given by

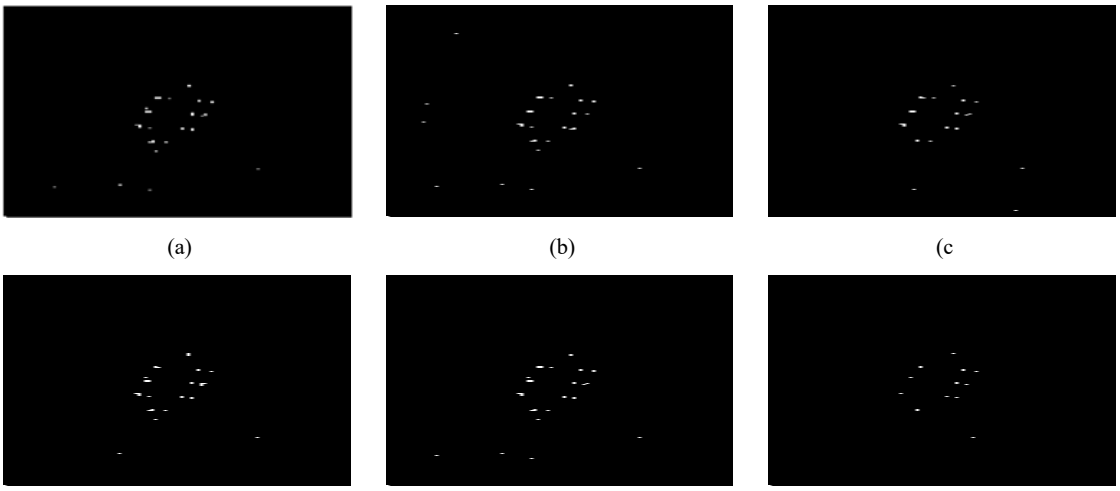

Fig. 6. Detection results (a) CA-CFAR, (b) 2P-CFAR, (c) GOCA-CFAR, (d) OS-CFAR, (e) VIE-CFAR and (f) G0-CFAR

Table II. Results of detection methods (CFAR window size: 15×15 pixels, clutter depth: 2 pixels)

method	N_c	N_d	N_{fa}	P_d	$P_{fa\,out}$	*FOM*
CA-CFAR	1758210	51	175	0.82	0.0001	0.215
2P-CFAR	1758210	42	175	0.68	0.0001	0.177
SOCA-CFAR	1758210	2	175	0.11	0.0001	0.084
GOCA-CFAR	1758210	45	175	0.73	0.0001	0.190
OS-CFAR	1758210	54	175	0.87	0.0001	0.227
VIE-CFAR	1758210	54	175	0.87	0.0001	0.227
G0-CFAR	1758210	31	175	0.50	0.0001	0.131

$$P_{fa} = \frac{N_{fa}}{N_c} \tag{14}$$

Where N_{fa} is the number of false alarms.

The figure of merit is defined as follows

$$FOM = \frac{N_d}{N_t + N_{fa}} \tag{15}$$

As it can be seen in Table II, for a fixed probability of 0.0001, the OS-CFAR and VIE-CFAR methods have a better probability of detection and figure of merit. CA-CFAR is in the next rank. Fig. 7 shows the receiver operating characteristic curve (ROC) for these methods. In this figure, the probability of

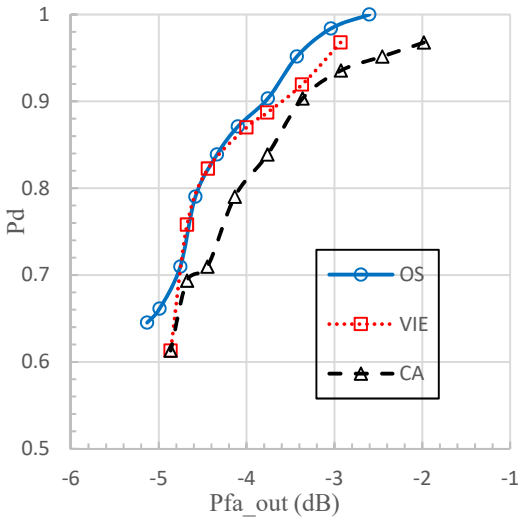

Fig. 7. ROC curves of three detectors (Pd vs. Pfa_out)

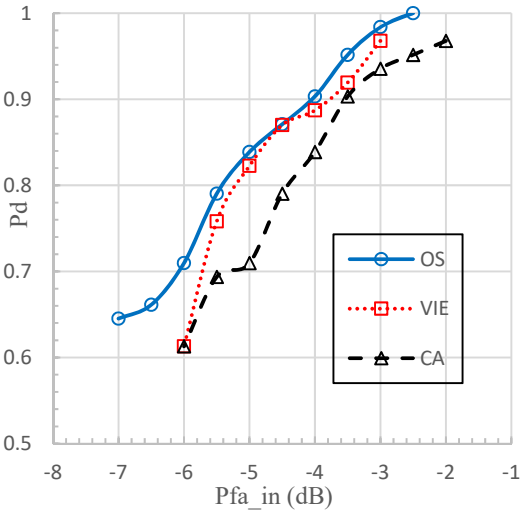

Fig. 8. ROC curves of three detectors (Pd vs. Pfa_in)

Table III. Results of detection for four simulated images (CFAR window size: 15×15 pixels, clutter depth: 2 pixels)

Image ID	Azimuth shift (m)	Range shift (m)	OS-CFAR		VIE-CFAR		CA-CFAR	
			N_d	P_d	N_d	P_d	N_d	P_d
1	2000	2000	54	0.87	54	0.87	51	0.82
2	1000	1000	45	0.59	38	0.50	34	0.44
3	500	500	35	0.41	23	0.27	29	0.34
4	0	0	45	0.51	34	0.39	30	0.34

detection is drawn in terms of the output probability of false alarm (Pfa_out), which is actually calculated after the completion of the detection task. Instead, one can draw the probability of detection in terms of the input probability of false alarm (Pfa_in), which is the desired probability of false alarm. The latter is shown in Fig. 8. It can be seen from Fig. 7 and Fig. 8 that OS-CFAR has better detection performance than VIE-CFAR and CA-CFAR for almost all input and output probabilities of false alarm.

Table III shows detection results of three more simulated images for OS-CFAR, VIE-CFAR, and CA-CFAR. The results of the previous image are also brought here for comparison. These images are different in the values of target azimuth and range shifts related to the flight path of the SAR platform. The probability of false alarm is fixed and equal to 0.0001. Again, we can see that OS-CFAR is the best in terms of probability of detection. Fig. 9 shows simulated images and detection results of OS-CFAR for images with ID numbers of 2, 3, and 4. The ROC curves for these three new simulated images are drawn in Fig. 10 and Fig. 11. It is clear that OS-CFAR has better performance in all

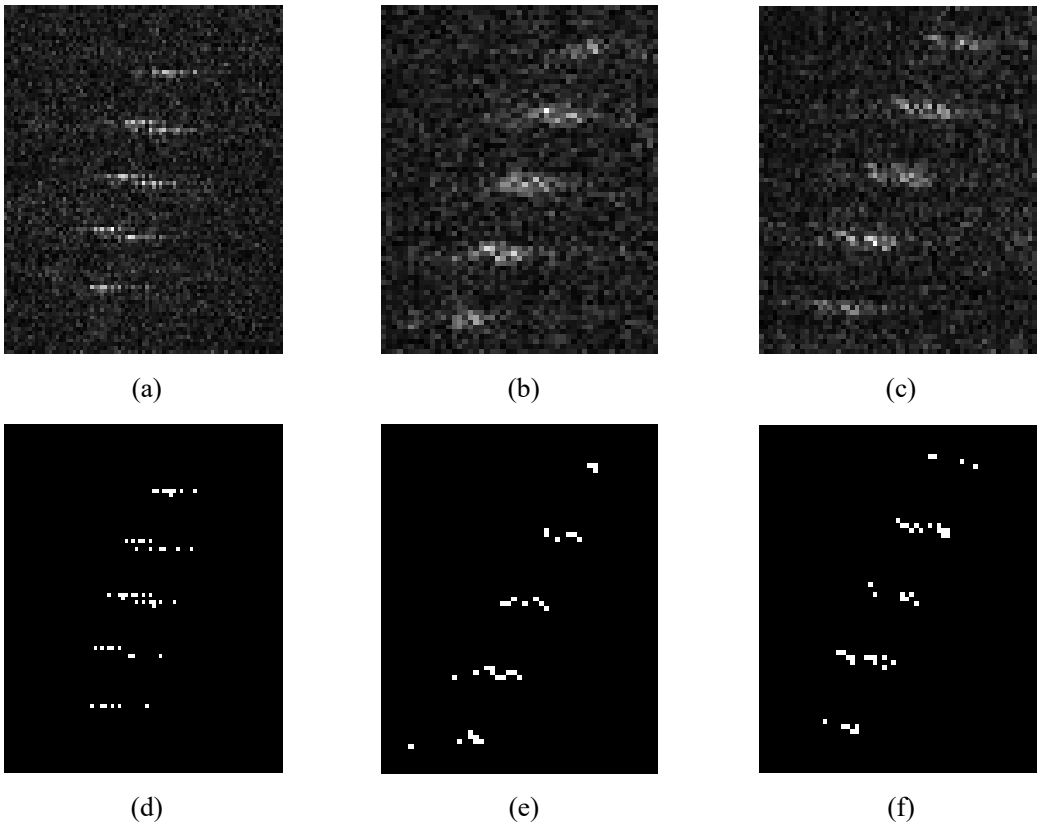

Fig. 9. (a) Simulated image number 2, (b) Simulated image number 3, (c) Simulated image number 4, (d) OS-CFAR detection result of image 2, (e) OS-CFAR detection result of image 3, (f) OS-CFAR detection result of image 4

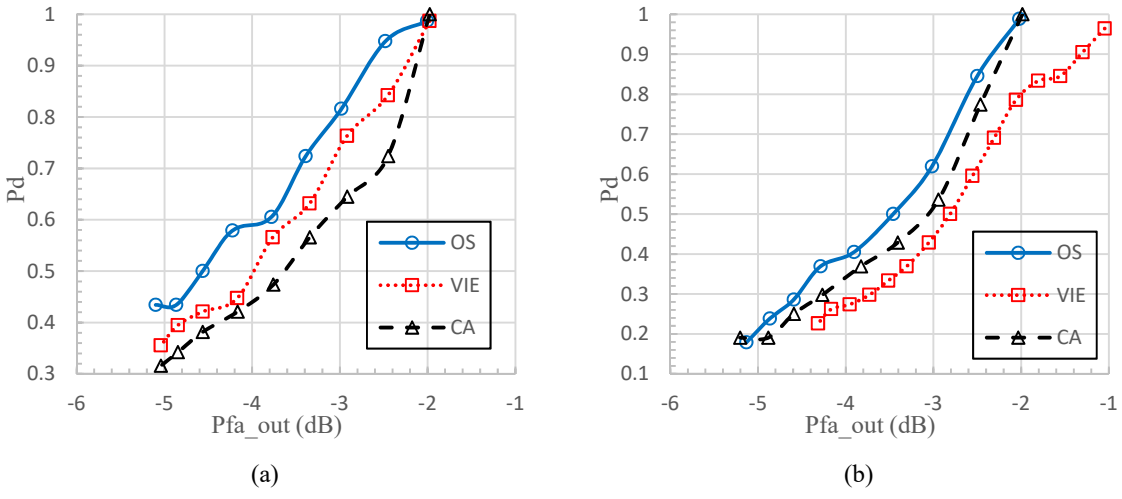

Fig. 10. ROC curves of three detection methods (a) Image 2, (b) Image 3

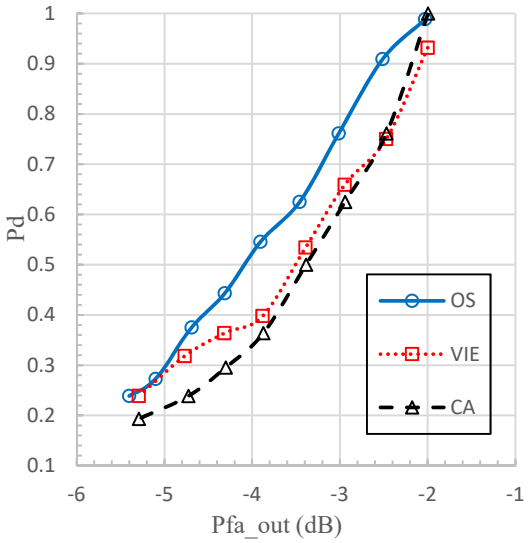

Fig. 11. ROC curve for Image 4

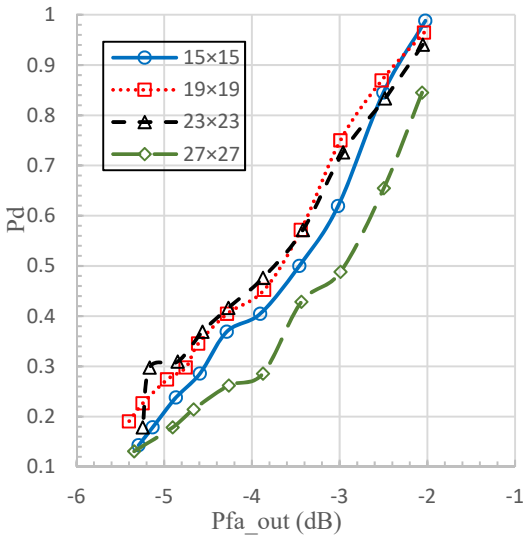

Fig. 12. ROC curve of OS-CFAR detection result of image 3 for different sizes of CFAR window

images. But as the target gets closer to the flight path of the SAR platform, the azimuth resolution gets worse, the scatterers spread over multiple cells, the homogeneity of the clutter area of the CFAR window is corrupted by some target pixels, and finally, as a result, the probability of detection degrades. One solution to this problem is to change the size of the CFAR window. Fig. 12 shows ROC curve of OS-CFAR detection of image 3 for different sizes of CFAR window. As it can be seen, a CFAR window size of 23×23 pixels has a better probability of detection for false alarm probability of 0.0001.

IV. CONCLUSION

In an attempt to find an appropriate solution for sea target detection in HSP-FLSAR, a variety of basic traditional CFAR detectors, including CA-CFAR, GOCA-CFAR, SOCA-CFAR, 2P-CFAR, and OS-CFAR, in addition to VIE-CFAR, which is an intelligent combination of other methods, and G0-CFAR, which is a better modelling of clutter, are used. All algorithms are implemented in software and applied to simulated HSP-FLASAR images. The images are different in their distance to SAR platform flight path. Detection results are compared based on receiver characteristic curves. The results show that OS-CFAR has the best probability of detection for a fixed input and output probability of false alarm. Also, the detection performance of OS-CFAR for near flight path targets can be improved by using bigger CFAR window.

REFERENCES

[1] J. Saeedi, "Feasibility Study and Conceptual Design of Missile-Borne Synthetic Aperture Radar," *IEEE Trans. Syst., Man, Cybern. Syst.*, vol. 50, no. 3, pp. 1122-1133, March 2020.

[2] P. Guo, S. Tang, L. Zhang, et al., "Improved focusing approach for highly squinted beam steering SAR," *IET Radar Sonar Navig*., vol. 10, no. 8, pp.1394-1399, March 2016.

[3] C. Hongmeng, L. Yaobing, M. Heqiang, et al., "Efficient forward-looking imaging via synthetic bandwidth azimuth modulation imaging radar for high-speed platform," *Sig. Process*., vol. 138, pp. 63-70, March 2017.

[4] D. J. Crisp, "The state-of-the-art in ship detection in synthetic aperture radar imagery," *DSTO Info. Sci. Lab*., May 2004.

[5] K. El-Darymli, P. McGuire, D. Power, et al., "Target detection in synthetic aperture radar imagery: A state-of-the-art survey," *J. Appl. Rem. Sens.*, vol. 7, no. 1, p. 71598, May 2013.

[6] B. Magaz, A. Beloucherani, M. Hamadouche, "Automatic threshold selection in OS-CFAR radar detection using information theoretic criteria," *Prog. Electromag. Res. B*, vol. 30, pp.157-175, May 2011.

[7] J. Kefeng, X. Xiangwei, Z. Huanxin, et al., "A novel variable index and excision CFAR based ship detection method on SAR imagery," *J. Sens.*, pp. 1-10, 2015.

[8] G. Gao, "Statistical modelling of SAR images: a survey," *Sensors*, vol. 10, pp. 775-795, 2010.

[9] G. Gao, S. Gao, J. Ouyang, et al, "Scheme for characterizing clutter statistics in SAR amplitude images by combining two parametric models," IEEE *Trans. Geosci. Rem. Sens.*, vol. 56, no. 10, pp. 5636-5646, 2018.

[10] G. G. Acosta, S. A. Villar, "Accumulated CA-CFAR process in 2-D for online object detection from sidescan sonar data," *IEEE J. Ocean. Eng.*, vol. 40, no. 3, pp. 558-569, 2015.

[11] S. Meng, K. Ren, D. Lu, et al., "A novel ship CFAR detection algorithm based on adaptive parameter enhancement and wake-aided detection in SAR images," *Infra. Phys. Tech.*, vol. 89, pp. 263-270, 2018.

[12] M. A. Richards, *Fundamentals of radar processing,* 2nd Edition, Mcgraw-Hill, 2014, ch. 7, pp. 364-374

[13] G. Gao, L. Liu, L. Zhao, et al., "An adaptive and fast CFAR algorithm based on automatic censoring for target detection in high-resolution SAR images," *IEEE Trans. Geosci. Rem. Sens.*, vol. 47, no. 6, pp. 1685-1697, 2009.

[14] G. Gao, *Characterizing of SAR clutter and its application to land and ocean observations*, Springer-Verlag, 2019, ch. 2, pp 53-70

[15] R. Toreinia, M. Kazerooni, M. Fallah, "A novel method in sea clutter and target simulation of forward-looking synthetic aperture radar," *J. Appl. Electromag. (in Persian)*, vol. 4, no. 1, pp. 9-20, 2016.

[16] X. Leng, K. Ji, X. Xing, et al., "Area ratio invariant feature group for ship detection in SAR Imagery" *IEEE J. Sel. Top. Appl. Earth Observ. Rem. Sens.*, vol. 11, no. 7, pp. 2376-2388, 2018.